fractal and fractional

MDPI

Article

Theoretical and Experimental Designs of the Planetary Boundary Layer Dynamics through a Multifractal Theory of Motion

Marius Mihai Cazacu [1], Iulian-Alin Roșu [2,*], Luminița Bibire [3], Decebal Vasincu [4], Ana Maria Rotundu [2] and Maricel Agop [1,5,*]

[1] Department of Physics, "Gheorghe Asachi" Technical University of Iasi, 700050 Iaşi, Romania
[2] Faculty of Physics, "Alexandru Ioan Cuza" University of Iasi, 700506 Iaşi, Romania
[3] Department of Environmental Engineering and Mechanical Engineering, Faculty of Engineering, Vasile Alecsandri University of Bacau, 600115 Bacău, Romania
[4] Department of Biophysics, Faculty of Dental Medicine, "Grigore T. Popa" University of Medicine and Pharmacy, 700115 Iaşi, Romania
[5] Academy of Romanian Scientists, 050044 Bucharest, Romania
* Correspondence: alin.iulian.rosu@gmail.com (I.-A.R.); m.agop@yahoo.com (M.A.)

Abstract: The accurate determination of atmospheric temperature with telemetric platforms is an active issue, one that can also be tackled with the aid of multifractal theory to extract fundamental behaviors of the lower atmosphere, which can then be used to facilitate such determinations. Thus, in the framework of the scale relativity theory, PBL dynamics are analyzed through the aid of a multifractal hydrodynamic scenario. Considering the PBL as a complex system that is assimilated to mathematical objects of a multifractal type, its various dynamics work as a multifractal tunnel effect. Such a treatment allows one to define both a multifractal atmospheric transparency coefficient and a multifractal atmospheric reflectance coefficient. These products are then employed to create theoretical temperature profiles, which lead to correspondences with real results obtained by radiometer data (RPG-HATPRO radiometer), with favorable results. Such methods could be further used and refined in future applications to efficiently produce atmospheric temperature theoretical profiles.

Keywords: PBL dynamics; multifractality; scale relativity theory; radiometer data

Citation: Cazacu, M.M.; Roșu, I.-A.; Bibire, L.; Vasincu, D.; Rotundu, A.M.; Agop, M. Theoretical and Experimental Designs of the Planetary Boundary Layer Dynamics through a Multifractal Theory of Motion. *Fractal Fract.* **2022**, *6*, 747. https://doi.org/10.3390/fractalfract6120747

Academic Editor: António Lopes

Received: 10 November 2022
Accepted: 15 December 2022
Published: 19 December 2022

1. General Considerations: From Differentiability to Non-Differentiability in Atmospheric Process Dynamics

The PBL (planetary boundary layer) dynamics remain a subject of great interest due to the many consequences regarding atmospheric behavior on both a local and a global scale. Because of the effects of buoyancy, tropospheric temperature profiles limits the motion verticality of atmospheric entities, and therefore the PBL appears as a principal stable factor in atmospheric dynamics [1]. The PBL is often turbulent, and because turbulence causes mixing, the bottom part of the standard atmosphere homogenizes, while the area above is commonly known as the "free atmosphere". Therefore, the PBL plays a tremendous role in aerosol and humidity transport and in the stratification and complex dynamic interplay of the atmosphere; its existence is commonly determined by inversions of various physical parameters, especially temperature [1]. However, while its common behavior patterns can be somewhat anticipated from a phenomenological perspective, the exact description of the atmospheric parameter inversions is not fully known.

Most models employed in the study of PBL dynamics assume, which can be unjustified, physical variables' differentiability. The successful applications of such models have to be understood on a sequential level, which means that differentiability would mostly be valid for larger domains. Classically, any and all dynamic variables that are dependent on spatiotemporal coordinates also become dependent on the scale resolution [1–5]. Thus,

instead of employing dynamical variables through non-differentiable functions, we must use certain approximations of that function derived through its averaging at different scale resolutions. As a consequence, all dynamic variables must then act as the limit of a family of functions, these being non-differentiable for a null scale resolution and differentiable for a nonzero scale resolution.

In general, non-differential methods are considered suitable in the field of complex systems, where real measurements are conducted at a finite scale resolution. The implication is that a new physical theory for such systems is developed, and in this theory, motion laws, which are invariant to coordinate transformations, must be integrated with scale laws that are similarly invariant. The present assumptions lead to a theory that was first developed in the framework of the scale relativity theory, which defines fractal physical models [4–6].

In the following, the PBL dynamics in the framework of the scale relativity theory are analyzed, assimilating it with a mathematical object of multifractal type (PBL dynamics considered through the multifractal tunnel effect). The rationale for this assimilation lies in the fact that the stratification of the lower atmosphere resembles the structure of a tunneling barrier scenario. The intent of this development is to continue the theoretical and practical advances into atmospheric physics using multifractality and to elaborate the basis of a multifractal theoretical model, which could be used to study the evolution of many types of parameters, most relevantly temperature. Starting with main theoretical aspects, the atmosphere is considered from a multifractal perspective, with all the mathematical consequences that this entails. Then, a multifractal tunnel effect in an external scalar potential configuration is seen to produce a multifractal barrier object, which plays the role of the PBL. This barrier entity and its properties are explained, and a variable is chosen which can function as an iterative parameter in order to implement the resulting equations as a model of atmospheric temperature. Finally, ceilometer and radiometer data are employed as experimental data, and theoretical atmospheric temperature data is contrasted with atmospheric temperature experimental data.

Regarding the usage of the multifractal tunnel effect as a theoretical implement in atmospheric studies, to the best of our knowledge, this is a novel application; however, this effect was previously employed in a study explaining the "chameleon effect" of cholesterol [7]. In terms of merely applying multifractal theories to the atmosphere, a number of studies have been elaborated, such as one that deals with developing a multifractal random-walk description of turbulence itself, another study that analyzes the multifractal long-term characteristics of local temperature fluctuations, and a recent study that seeks to multifractally characterize atmospheric particular matter pollution [8–10]. It is noteworthy, however, that given the theoretical complexity of using multifractal techniques, especially in a scientific field such as atmospheric studies, which is already marked by added difficulties in the form of chaos and scaling issues, there are not many current works that explore the connections between multifractality and atmospheric fluid dynamics. This is the case even though the formation of turbulence through strange attractors, which are fractal in nature, has been both experimentally and theoretically established decades ago [11,12]. Therefore, it is also our hope that this study will not only present a functional application of theory to practice but will also broaden the field of multifractal atmospheric study.

2. Theoretical Design: Non-Differentiability Calibrated on PBL Dynamics in the Form of the Multifractal Hydrodynamic Model

Considering the PBL's complexity, which can be assimilated with a mathematical object of multifractal type, in such conjecture, the PBL dynamics can be explained through the scale relativity theory (the PBL structural units occur on continuous but non-differentiable multifractal curves), dynamics that can be described through the scale covariance derivative [5,13–16]:

$$\frac{\hat{d}}{dt} = \partial_t + \hat{V}^l \partial_l + \frac{1}{4}(dt)^{\left[\frac{2}{f(\alpha)}\right]-1} D^{lp} \partial_l \partial_p \quad (1)$$

where:

$$\hat{V}^l = V_D^l - iV_F^l, \tag{2a}$$

$$D^{lp} = d^{lp} - i\hat{d}^{lp}, \tag{2b}$$

$$d^{lp} = \lambda_+^l \lambda_+^p - \lambda_-^l \lambda_-^p, \tag{2c}$$

$$\hat{d}^{lp} = \lambda_+^l \lambda_+^p + \lambda_-^l \lambda_-^p, \tag{2d}$$

$$\partial_t = \frac{\partial}{\partial t},\ \partial_l = \frac{\partial}{\partial x^l},\ \partial_l \partial_p = \frac{\partial}{\partial x^l}\frac{\partial}{\partial x^p},\ i = \sqrt{-1},\ l, p = 1, 2, 3. \tag{2e}$$

The meanings of the above parameters are explained in greater detail in one of our previous works [16].

There exist many types of ways to define the notion of fractal dimension: Kolmogorov fractal dimension, Hausdorff–Besikovitch fractal dimension, and many others [17–20]. For such studies, it is necessary to select just one of these definitions, and for the meaning of fractal dimension to be constant, given the fact that the dimension directly dictates whether or not the process is correlative or not [17–20]. Thus, through the singularity spectrum, $f(\alpha)$, it is possible to identify not only dynamic spaces in the PBL that are characterized by just one fractal dimension but also dynamic spaces whose fractal dimensions are situated in an interval of values, implying multifractality. It is possible to employ the singularity spectrum in order to identify universality classes in PBL dynamics, even considering the regularity of the attractors involved.

If the PBL dynamics are described by Markovian stochastic processes [21–23]:

$$\lambda_+^i \lambda_+^l = \lambda_-^i \lambda_-^l = 2\lambda\delta^{il} \quad i,\ l = 1,\ 2,\ 3, \tag{3}$$

where λ is a specific coefficient of the multifractal–non-multifractal scale transition and δ^{il} is Kronecker's pseudotensor, the scale covariant derivative in Equation (1) becomes:

$$\frac{d}{dt} = \partial_t + \hat{V}^l \partial_l - i\lambda (dt)^{\left(\frac{2}{f(\alpha)}\right)-1} \partial_l \partial^l. \tag{4}$$

Thus, if one accepts the principle of the scale covariance, which is by applying Equation (1) to Equation (2a), without constraints, the PBL's motion equations of the structural units dynamics become:

$$\frac{d\hat{V}^i}{dt} = \partial_t \hat{V}^i + \hat{V}^l \partial_l \hat{V}^i + \frac{1}{4}(dt)^{\left[\frac{2}{f(\alpha)}\right]-1} D^{lk} \partial_l \partial_k \hat{V}^i = 0. \tag{5}$$

In this manner, acceleration, $\partial_t \hat{V}^i$, convection, $\hat{V}^l \partial_l \hat{V}^i$, and dissipation, $D^{lk}\partial_l \partial_k \hat{V}^i$, are all balanced at every point of any multifractal curve of the PBL structural units dynamics. Particularly, for Equation (3), the motion Equation (5) becomes:

$$\frac{\hat{d}\hat{V}^i}{dt} = \partial_t \hat{V}^i + \hat{V}^l \partial_l \hat{V}^i - i\lambda (dt)^{\left[\frac{2}{D_F}\right]-1} \partial_l \partial^l \hat{V}^i = 0. \tag{6}$$

Now, through the separation of PBL structural units dynamics on scale resolution (differentiable and non-differentiable scale resolutions), Equation (5) becomes:

$$\partial_t V_D^i + V_D^l \partial_l V_D^i - V_F^l \partial_l V_F^i + \frac{1}{4}(dt)^{\left[\frac{2}{f(\alpha)}\right]-1} D^{lk} \partial_l \partial_k V_D^i = 0, \tag{7a}$$

$$\partial_t V_F^i + V_F^l \partial_l V_D^i + V_D^l \partial_l V_F^i - \frac{1}{4}(dt)^{\left[\frac{2}{f(\alpha)}\right]-1} D^{lk} \partial_l \partial_k V_F^i = 0, \tag{7b}$$

while Equation (6) takes the form:

$$\partial_t V_D^i + V_D^l \partial_l V_D^i - \left[V_F^l + \lambda (dt)^{\left[\frac{2}{f(\alpha)}\right]-1} \partial^l\right] \partial_l V_F^i = 0, \tag{8a}$$

$$\partial_t V_F^i + V_D^l \partial_l V_F^i + \left[V_F^l + \lambda (dt)^{[\frac{2}{f(\alpha)}]-1} \partial^l \right] \partial_l V_D^i = 0. \tag{8b}$$

For the non-rotational motions of the PBL structural units dynamics, the complex velocity fields in Equation (2a) take the form:

$$\hat{V}^i = -2i\lambda (dt)^{[\frac{2}{f(\alpha)}]-1} \partial^i ln\Psi, \tag{9}$$

where Ψ is the states function. From here, for:

$$\Psi = \sqrt{\rho} e^{is}, \tag{10}$$

where $\sqrt{\rho}$ is the amplitude and s is the phase, the complex velocity fields in Equation (9) become explicitly:

$$\hat{V}^i = 2\lambda (dt)^{[\frac{2}{f(\alpha)}]-1} \partial^i s - i\lambda (dt)^{[\frac{2}{f(\alpha)}]-1} \partial^i \ln \rho, \tag{11}$$

which enable the definition of the real velocity fields:

$$V_D^i = 2\lambda (dt)^{[\frac{2}{f(\alpha)}]-1} \partial^i s, \tag{12}$$

$$V_F^i = i\lambda (dt)^{[\frac{2}{f(\alpha)}]-1} \partial^i \ln \rho. \tag{13}$$

Through Equations (12) and (13) and using the mathematical procedures from [21–23], Equation (8) reduces to the multifractal hydrodynamic equations:

$$\partial_t V_D^i + V_D^l \partial_l V_D^i = -\partial^i Q, \tag{14}$$

$$\partial_t \rho + \partial_l \left(\rho V_D^l \right) = 0, \tag{15}$$

with Q, the multifractal specific potential:

$$Q = -2\lambda^2 (dt)^{[\frac{4}{f(\alpha)}]-2} \frac{\partial^l \partial_l \sqrt{\rho}}{\sqrt{\rho}} = -V_F^i V_F^i - \frac{1}{2} \lambda (dt)^{[\frac{2}{f(\alpha)}]-1} \partial_l V_F^l. \tag{16}$$

Equation (14) gives the multifractal specific momentum conservation law of the PBL dynamics, while Equation (15) produces the multifractal state density conservation law of the same dynamics. The multifractal specific potential in Equation (16) implies the multifractal specific force:

$$F^i = -\partial^i Q = -2\lambda^2 (dt)^{[\frac{4}{f(\alpha)}]-2} \partial^i \frac{\partial^l \partial_l \sqrt{\rho}}{\sqrt{\rho}}, \tag{17}$$

which shows the multifractality of the motion curves of the PBL dynamics.

We note that for external constraints, for example, the external scalar potential, U, the multifractal hydrodynamic equations take the form:

$$\partial_t V_D^i + V_D^l \partial_l V_D^i = -\partial^i (Q + U), \tag{18}$$

$$\partial_t \rho + \partial_l \left(\rho V_D^l \right) = 0. \tag{19}$$

It is possible to extrapolate the following theoretical results using the equations previously mentioned:

I. The existence of a multifractal specific force implies that all PBL structure units must be considered through a multifractal medium;
II. This medium can be considered a multifractal fluid whose dynamics are characterized by the hydrodynamic model presented previously;

III. Since the velocity field, V_F^i, is absent from the multifractal states density conservation laws, it induces the possibility of non-manifest PBL dynamics, meaning that it facilitates the transmission of multifractal specific momentum and multifractal energy;
IV. All potential issues regarding reversibility and existence of the eigenstates are solved by the conservation of multifractal energy and multifractal momentum;
V. When using the tensor:

$$\hat{\tau}^{il} = 2\lambda^2 (dt)^{\left[\frac{4}{f(\alpha)}\right]-2} \rho \partial^i \partial^l \ln \rho, \tag{20}$$

the multifractal specific potential (Q) equation can be defined as a multifractal equilibrium equation:

$$\rho \partial^i Q = \partial_l \hat{\tau}^{il}. \tag{21}$$

The multifractal tensor $\hat{\tau}^{il}$ can now be written in the form:

$$\hat{\tau}^{il} = \eta \left(\partial_l V_F^i + \partial_i V_F^l \right), \tag{22}$$

with:

$$\eta = \lambda (dt)^{\left[\frac{2}{f(\alpha)}\right]-1} \rho. \tag{23}$$

Then, this is a multifractal linear constitutive equation that must be employed for a multifractal "viscous fluid".

3. PBL Dynamics Mimed as a Multifractal Atmospheric Tunnel Effect

Let us describe the PBL dynamics through the following assumptions:

I. The PBL, as a complex system both in a structural and functional perspective, can be assimilated with a mathematical object of multifractal type;
II. PBL dynamics can be described through the scale relativity theory in the form of multifractal hydrodynamic equations;
III. The PBL works as a multifractal atmospheric tunnel effect described through the external scalar potential (see Figure 1):

$$U(x) = \begin{cases} 0 & -\infty < x < 0 \\ U_0 & 0 \le x \le \mathrm{a} \\ 0 & \mathrm{a} < x < +\infty \end{cases}, \tag{24}$$

where U_0 is the multifractal atmospheric barrier height and a is its width (the characteristics of PBL).

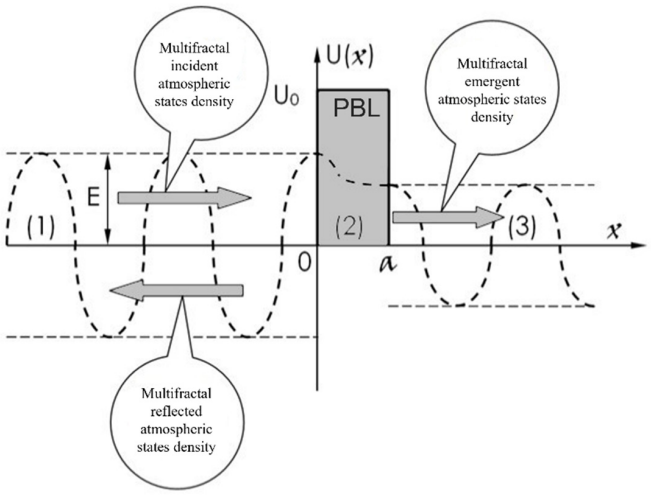

Figure 1. External scalar potential configuration (multifractal atmospheric barrier—PBL) for the tunnel effect of the multifractal (atmospheric) type.

Then, PBL dynamics are described through the multifractal energy conservation law of the form:

$$Q + U = E, \tag{25}$$

or explicitly:

$$2\lambda^2 (dt)^{\left[\frac{4}{f(\alpha)}\right]-2} \frac{\partial^l \partial_l \sqrt{\rho}}{\sqrt{\rho}} + U = E. \tag{26}$$

In Equation (26), ρ is the multifractal atmospheric state density, U is the external scalar potential, λ is the specific coefficient associated with the multifractal–non-multifractal transition, and E is the multifractal energy constant. We note that the results of Equation (26) are given by means of the functionality of the first Newton's principle applied to Equation (18) on multifractal manifolds.

Considering the one-dimensional case, Equation (26) through the substitution:

$$\sqrt{\rho} = \theta(x), \tag{27}$$

becomes:

$$\partial_{xx}\theta(x) + \frac{1}{2\lambda^2 (dt)^{\left[\frac{4}{f(\alpha)}\right]-2}} (E - U)\theta(x) = 0. \tag{28}$$

In the following, the above equations will be used to mime PBL dynamics through the multifractal atmospheric tunnel effect (any PBL structural unit with known energy penetrates a barrier of greater energy than the incident one).

As it is shown in Figure 1, we distinguish three zones denoted by (1), (2), and (3) as:

(1). the multifractal atmospheric incidence zone;
(2). the multifractal atmospheric barrier;
(3). the multifractal atmospheric emergence zone.

In such context, if θ_1, θ_2, and θ_3 are the multifractal functions corresponding to the above mentioned three zones, we have the following equations:

$$\frac{d^2\theta_1}{dx^2} + k^2\theta_1 = 0, \ -\infty < x < 0 \tag{29a}$$

$$\frac{d^2\theta_2}{dx^2} - q^2\theta_2 = 0, \ 0 \le x \le \mathrm{a} \tag{29b}$$

$$\frac{d^2\theta_3}{dx^2} + k^2\theta_3 = 0, \ \mathrm{a} < x < +\infty \tag{29c}$$

where:

$$k^2 = \frac{E}{2\lambda^2 (dt)^{(4/f(\alpha))-2}}, q^2 = \frac{U_0 - E}{2\lambda^2 (dt)^{(4/f(\alpha))-2}} \tag{30}$$

Now, through integration, the following solutions of the above equations are obtained:

$$\theta_1(x) = A_1 e^{ikx} + B_1 e^{-ikx}, \ -\infty < x < 0 \tag{31a}$$

$$\theta_2(x) = A_2 e^{qx} + B_2 e^{-qx}, \ 0 \le x \le a \tag{31b}$$

$$\theta_3(x) = A_3 e^{ikx}, \ \mathrm{a} < x < +\infty \tag{31c}$$

where A_1, B_1, A_2, B_2, and A_3 are constants. We note the following:

I. e^{ikx} corresponds to the multifractal incident atmospheric states density (from $-\infty$) in the multifractal zone (1) and to the multifractal emergent atmospheric states density (to $+\infty$) in the multifractal zone (3);
II. e^{-ikx} corresponds to the multifractal reflected atmospheric states density, which exists only in the multifractal zone (1), passing from $x = 0$ to $x = -\infty$ since in the multifractal zone (3), the external scalar potential is uniformly null.

Since the general expression of the multifractal atmospheric current of the states density in the one-dimensional case has the form [5,24]:

$$J_x = i\lambda(dt)^{(2/f(\alpha))-1}\left(\theta\frac{d\bar{\theta}}{dx} - \bar{\theta}\frac{d\theta}{dx}\right) \tag{32}$$

then the following currents can be defined:

- The multifractal atmospheric current density of the multifractal atmospheric incident states density in zone (1):

$$J_i = 2\lambda(dt)^{\left(\frac{2}{f(\alpha)}\right)-1}k|A_1|^2 \tag{33}$$

- The multifractal atmospheric current density of the multifractal atmospheric emergent states density in zone (3):

$$J_e = 2\lambda(dt)^{(2/f(\alpha))-1}k|A_3|^2 \tag{34}$$

- The multifractal atmospheric current density of the multifractal reflected atmospheric states density:

$$J_r = -2\lambda(dt)^{(2/f(\alpha))-1}|B_1|^2 \tag{35}$$

These results give the possibility of a univocal characterization of the multifractal atmospheric tunnel effect through the multifractal atmospheric transparency:

$$T = \frac{J_e}{J_i} = \left|\frac{A_3}{A_1}\right|^2 \tag{36}$$

and the multifractal atmospheric reflectance:

$$R = \frac{J_r}{J_i} = \left|\frac{B_1}{A_1}\right|^2 \tag{37}$$

Imposing now the coupling conditions (in $x = 0$ and $x = a$), both for the functions θ_i and their derivates, i.e.,

$$\theta_1(0) = \theta_2(0) \tag{38a}$$

$$\frac{d\theta_1}{dx}(0) = \frac{d\theta_2}{dx}(0) \tag{38b}$$

$$\theta_2(a) = \theta_3(a) \tag{38c}$$

$$\frac{d\theta_2}{dx}(a) = \frac{d\theta_3}{dx}(a) \tag{38d}$$

the multifractal algebraic system is obtained:

$$A_1 + B_1 = A_2 + B_2 \tag{39a}$$

$$ik(A_1 - B_1) = q(A_2 - B_2) \tag{39b}$$

$$e^{qa}A_2 + e^{-qa}B_2 = e^{iqa}A_3 \tag{39c}$$

$$q\left(e^{qa}A_2 - e^{-qa}B_2\right) = ike^{iqa}A_3 \tag{39d}$$

Following the same mathematical procedure from [24], the multifractal atmospheric transparency takes the form:

$$T = \frac{4q^2k^2}{4q^2k^2 + (q^2+k^2)^2\mathrm{sh}^2(qa)} \tag{40}$$

while the multifractal atmospheric reflectance becomes:

$$R = \frac{\left(k^2 + q^2\right)^2}{\left(q^2 - k^2\right)^2 + 4q^2k^2 \cdot \mathrm{cth}^2(qa)} \tag{41}$$

Moreover, in the old notations (30), it is obtained:

$$R = \frac{U_0^2 \mathrm{sh}^2\left\{\left[\frac{(U_0 - E)}{2\lambda^2 (dt)^{(4/f(\alpha))-2}}\right]^{1/2} a\right\}}{U_0^2 \mathrm{sh}^2\left\{\left[\frac{(U_0 - E)}{2\lambda^2 (dt)^{(4/f(\alpha))-2}}\right]^{1/2} a\right\} + 4E(U_0 - E)} \tag{42}$$

$$T = \frac{4E(U_0 - E)}{U_0^2 \mathrm{sh}^2\left\{\left[\frac{(U_0 - E)}{2\lambda^2 (dt)^{(4/f(\alpha))-2}}\right]^{1/2} a\right\} + 4E(U_0 - E)} \tag{43}$$

For graphical dependencies, it is preferable to use the dimensionless coordinate system:

$$X = ka = \left[\frac{E}{2\lambda^2 (dt)^{\left(\frac{4}{f(\alpha)}\right)-2}}\right]^{\frac{1}{2}} a \tag{44a}$$

$$Y = qa = \left[\frac{(U_0 - E)}{2\lambda^2 (dt)^{(4/f(\alpha))-2}}\right]^{\frac{1}{2}} a \tag{44b}$$

Then, the multifractal atmospheric transparency and multifractal atmospheric reflectance become:

$$R = \frac{\left(X^2 + Y^2\right)^2}{\left(Y^2 - X^2\right)^2 + 4X^2Y^2\mathrm{cth}^2(Y)} \tag{45}$$

$$T = \frac{4X^2Y^2}{4X^2Y^2 + \left(X^2 + Y^2\right)^2 \mathrm{sh}^2(Y)} \tag{46}$$

The 3D variations of the multifractal atmospheric transparency, T, on the dimensionless coordinates, X and Y, are depicted in Figure 2a,b:

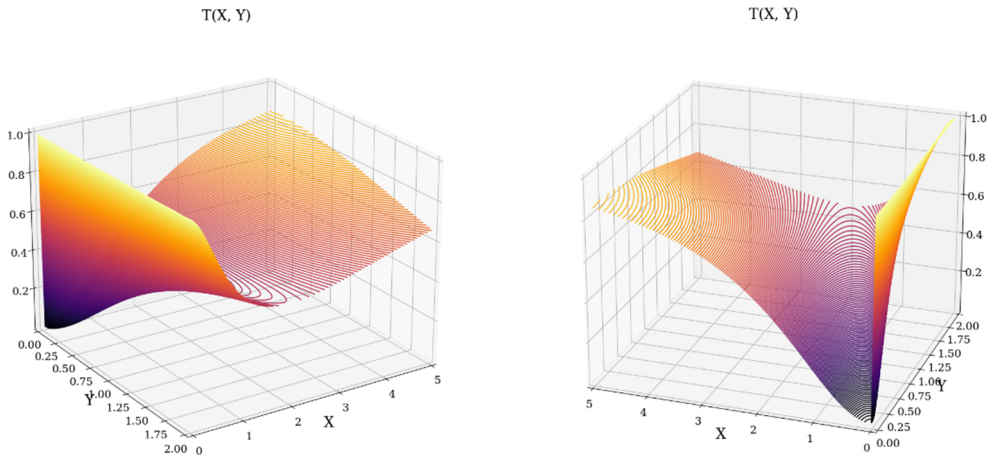

(**a**) (**b**)

Figure 2. The 3D variations of the multifractal atmospheric transparency, T, of the dimensionless coordinates, X and Y: (**a**,**b**) the dependence T = T (X, Y).

The 2D variations of the multifractal atmospheric transparency, T, on the dimensionless coordinates, X and Y, are depicted in Figure 3a,b:

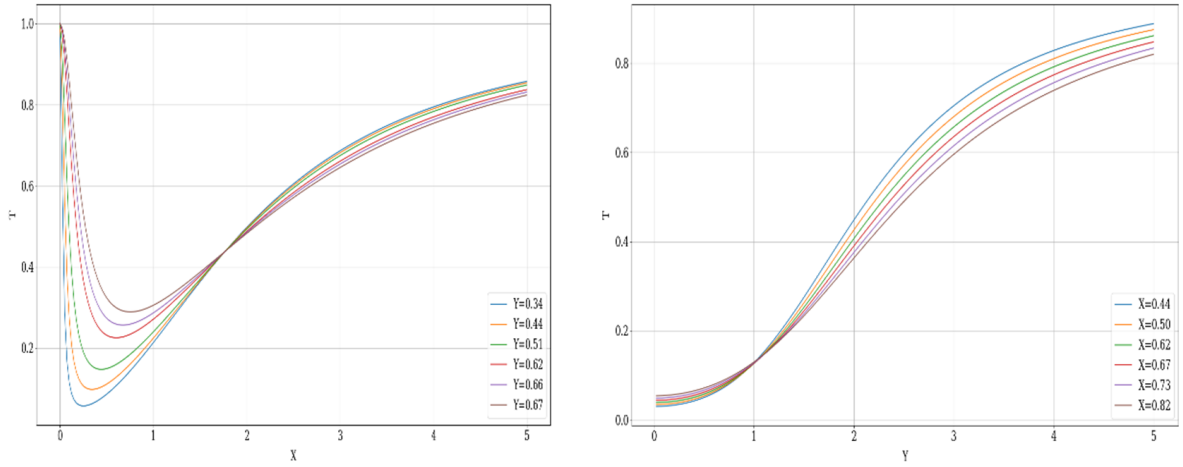

(**a**) (**b**)

Figure 3. The 2D variations of the multifractal atmospheric transparency, T, of the dimensionless coordinates, X and Y: (**a**) the dependence T = T (X, Y = constant); (**b**) the dependence T = T (X = constant, Y).

In Figure 4a,b, the 3D variations of the multifractal–atmospheric reflectance, R, on the dimensionless coordinates, X and Y, are given.

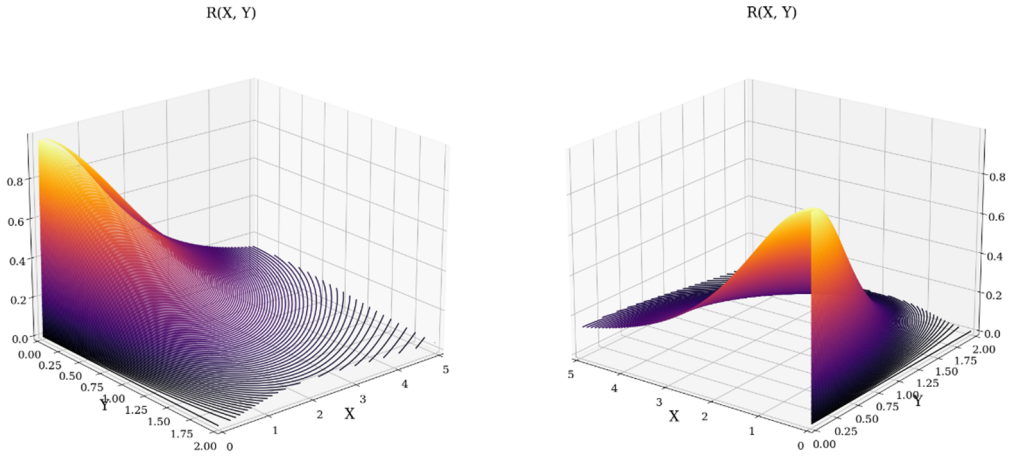

(**a**) (**b**)

Figure 4. The variation of the multifractal atmospheric reflectance, R, of the dimensionless coordinates, X and Y: (**a**,**b**) the dependence R = R (X, Y).

The dependence that T manifests with regards to X involves both minimal and asymptotic positive variations of the multifractal atmospheric transparency, while the dependence of T with regards to Y shows only asymptotic positive variations of this transparency. In the case of R, the behavior is exactly opposite, with the dependence that R manifests with regards to X involving maximal and asymptotic negative variations of the multifractal atmospheric reflectance, while the dependence of R with regards to Y involves only asymptotic negative variations of the multifractal atmospheric reflectance.

In Figure 5a,b, the 2D variations of the multifractal–atmospheric reflectance, R, on the dimensionless coordinates, X and Y, are given.

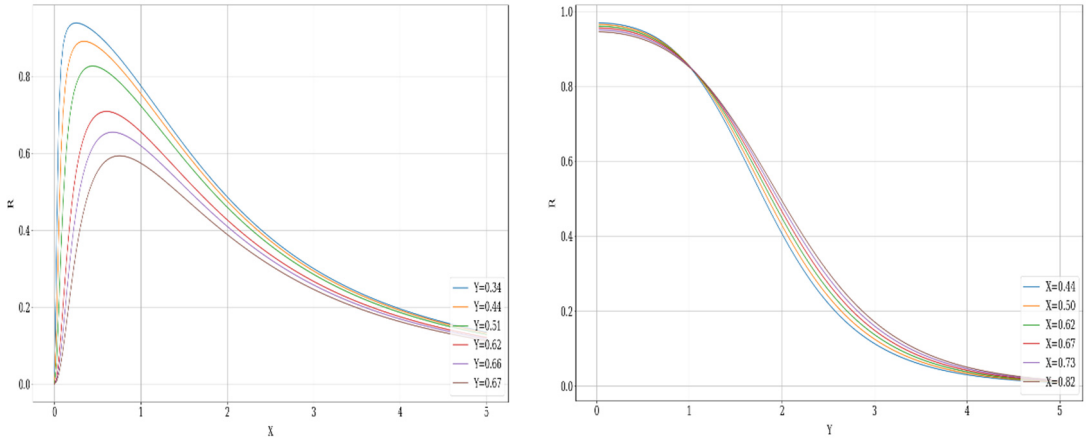

(**a**) (**b**)

Figure 5. The 2D variations of the multifractal atmospheric reflectance, R, of the dimensionless coordinates, X and Y: (**a**) the dependence R = R (X, Y = constant); (**b**) the dependence R = R (X = constant, Y).

In such a frame, since X is proportional with a minimal dimension relevant to the PBL, namely the potential barrier width a, and T has a proportionality relation with the atmospheric PBL temperature, Figure 3a can be transformed into Figure 6.

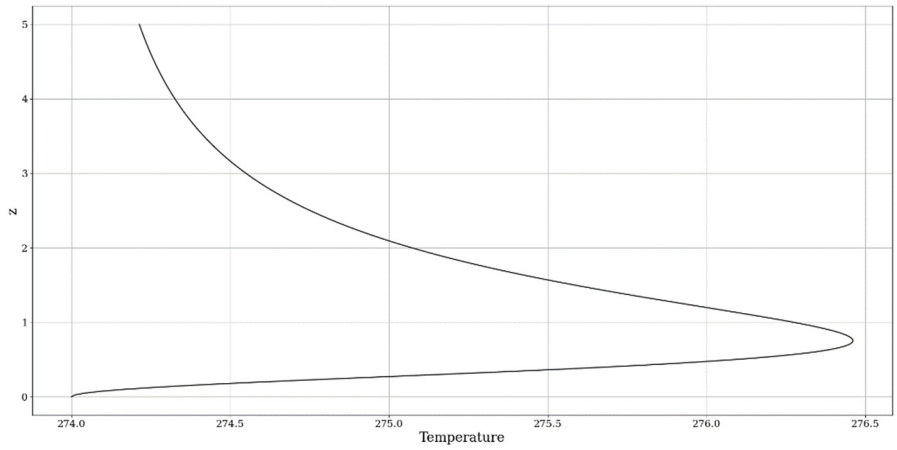

Figure 6. Example of a theoretical atmospheric temperature profile.

The theoretical results imply a temperature inversion, thus showing a good accord with a common understanding of the atmospheric temperature profile. Furthermore, with the decrease in transparency, a confined multifractal environment is created in the barrier, which then leads to a greater states density and an increase in temperature, which is in correspondence with the experimental results.

4. Experimental Design

For the purpose of confirming the reflectance and transparency results obtained so far, real atmospheric profiles are required. This profiling is justified by the fact that our analysis considers the PBL, and other atmospheric boundary layers, as multifractal barriers whose lengths represent their thickness relative to an atmospheric profile perpendicular to the ground level. Indeed, the fact that the non-dimensional parameters, X and Y, are proportional to the parameter a points to the fact that vertical atmospheric profiles represent the transport phenomena of multifractal atmospheric parameters through multifractal barriers. Ideally, to test the theories of transparency, an atmospheric parameter with a high degree of predictability and whose profile behaviors are relatively well known must be chosen, and atmospheric temperature proves itself to be an ideal candidate. When verifying

the inversion behavior of such a parameter, it is important to note that temperature has a natural connection to the states density in all non-degenerated-type systems. In addition, in our context, all multifractal physical measures are, in one way or another, proportional or inversely proportional to the transparency in the multifractal barrier. However, what also must be considered is that the equations for transparency and reflectance are non-dimensional, in which case the proportionality or inverse proportionality can vary in the way that it must be considered, and instead of perfect proportionality, patterns of behavior must be identified.

In order for our theoretical results to be compared to real data, theoretical temperature profiling must be achieved, and thus the transparency equation must be iterated as a model for the theoretical modeling of the atmospheric temperature, as in Figure 6. The control parameter of such a model, since we have considered the proportionality of X and Y to a, is the PBLH, which in this case can be considered synonymous with a itself. To obtain the PBLH, ceilometer data has been used, and temperature data has been obtained through radiometer data. The ceilometer platform utilized in this study is a CHM15k ceilometer operating at a 1064 nm wavelength, and the radiometer platform is an RPG-HATPRO radiometer platform. Both are positioned in Galați, Romania, at the UGAL–REXDAN facility found at coordinates 45.435125N, 28.036792E, 65 m ASL, which is a part of the "Dunărea de Jos" University of Galați. These instruments have been chosen and set up to conform to the standards imposed by the ACTRIS community. From a computational perspective, the necessary calculations are performed through code written and operated in Python 3.6. Four instances are chosen for this study: all four are time series taken on the 5th, 6th, 7th, and 8th of May 2022 (Figures 7–18). Static profiles are also shown, and all of them are extracted from the beginning of the time series (Figures 19–22).

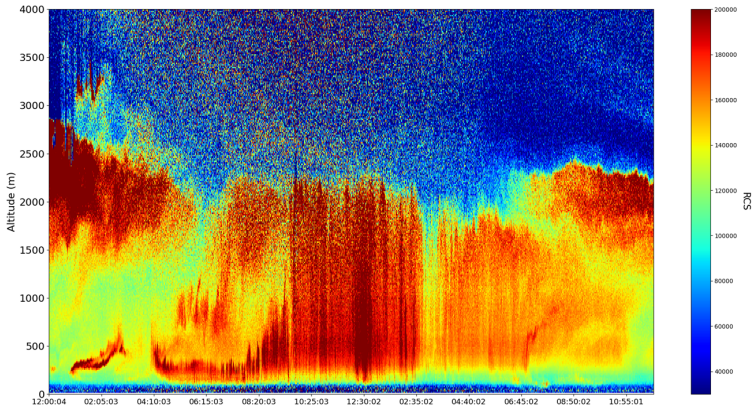

Figure 7. Time series of atmospheric RCS profiles; ceilometer data; Galati, Romania, 5 May 2022.

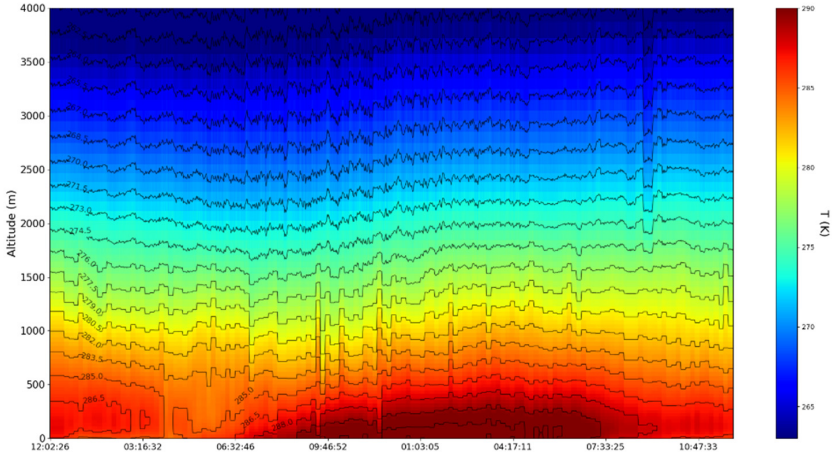

Figure 8. Time series of atmospheric temperature profiles; radiometer data; Galati, Romania, 5 May 2022.

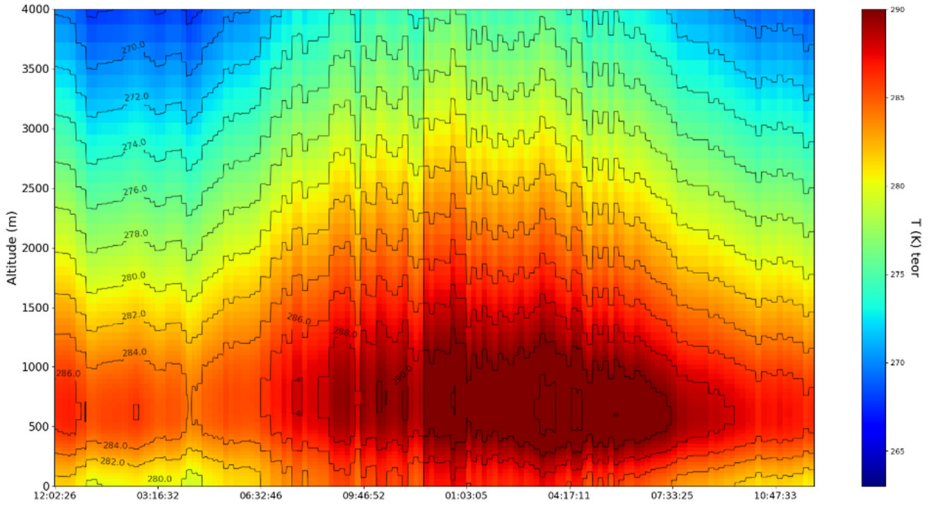

Figure 9. Time series of atmospheric temperature profiles; theoretical model data; Galati, Romania, 5 May 2022.

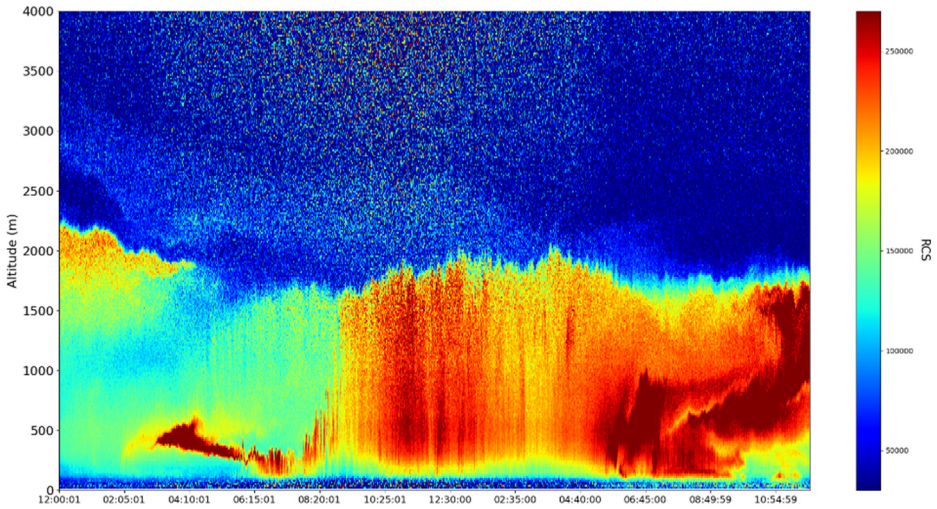

Figure 10. Time series of atmospheric RCS profiles; ceilometer data; Galati, Romania, 6 May 2022.

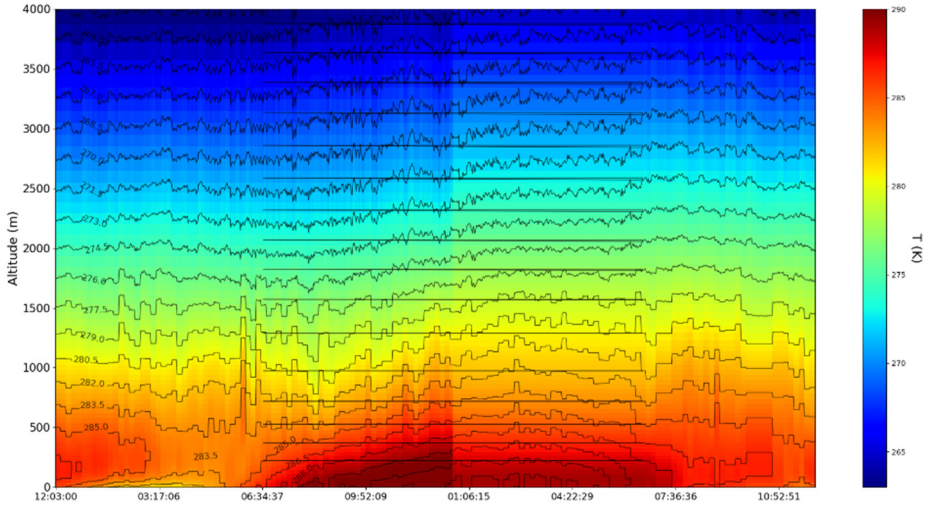

Figure 11. Time series of atmospheric temperature profiles; radiometer data; Galati, Romania, 6 May 2022.

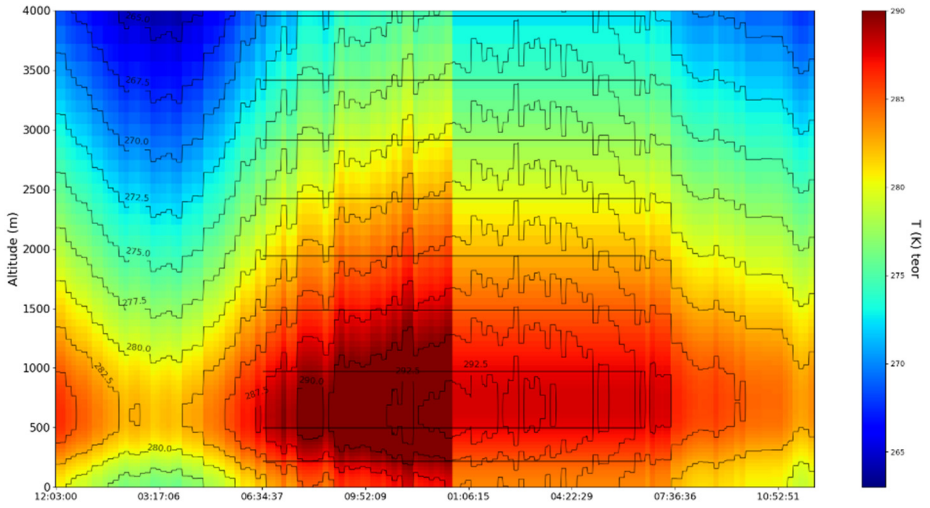

Figure 12. Time series of atmospheric temperature profiles; theoretical model data; Galati, Romania, 6 May 2022.

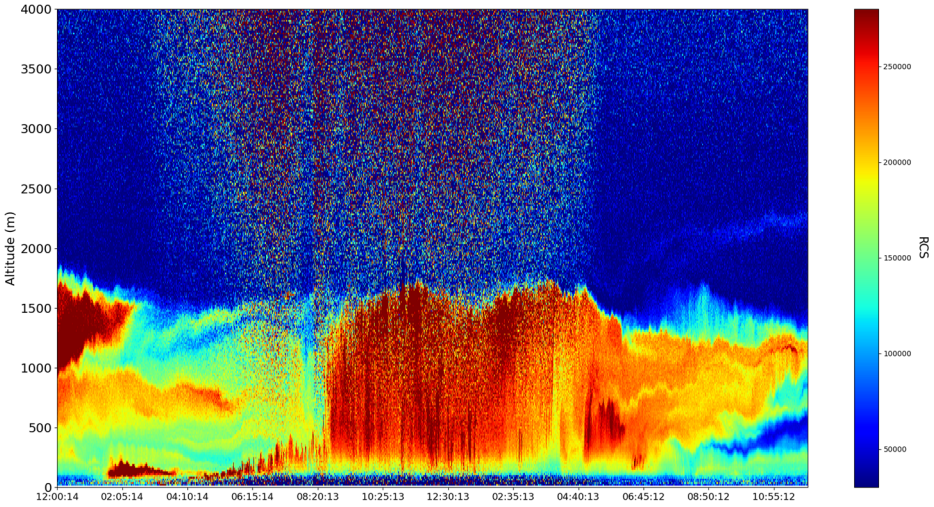

Figure 13. Time series of atmospheric RCS profiles; ceilometer data; Galati, Romania, 7 May 2022.

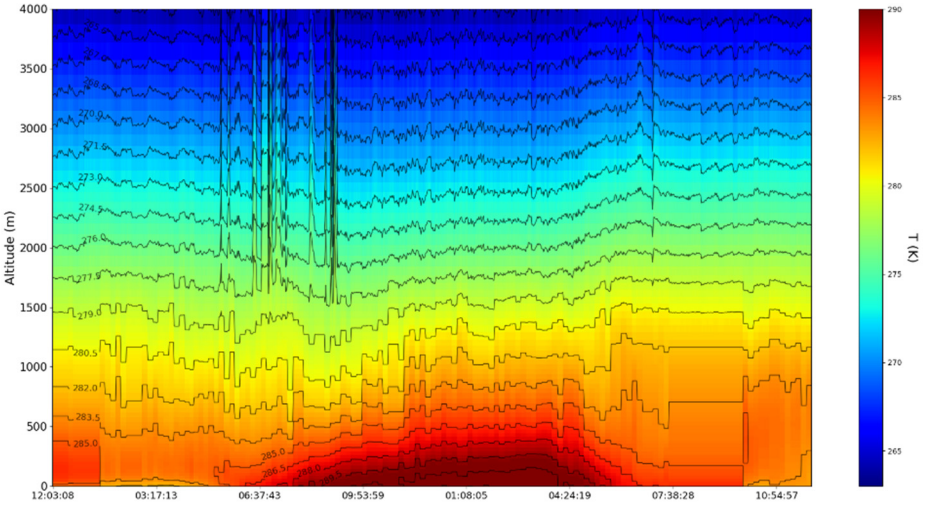

Figure 14. Time series of atmospheric temperature profiles; radiometer data; Galati, Romania, 7 May 2022.

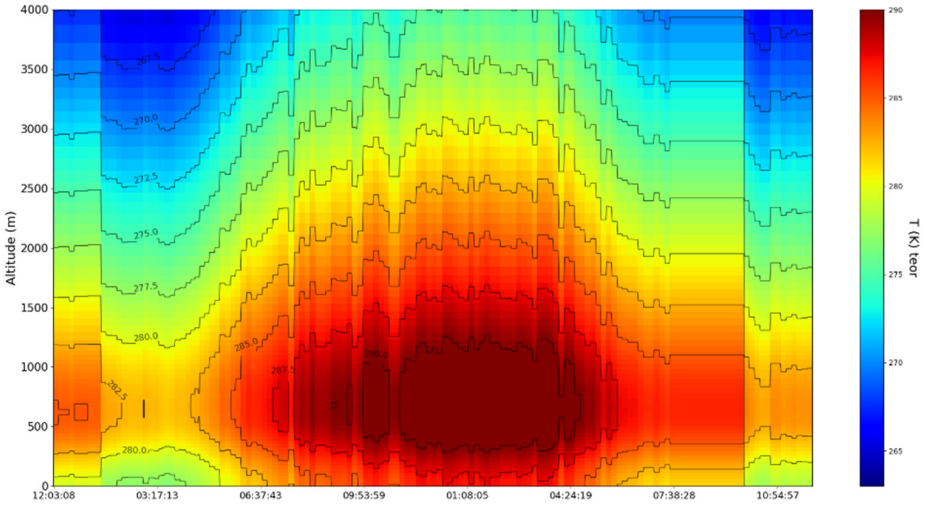

Figure 15. Time series of atmospheric temperature profiles; theoretical model data; Galati, Romania, 7 May 2022.

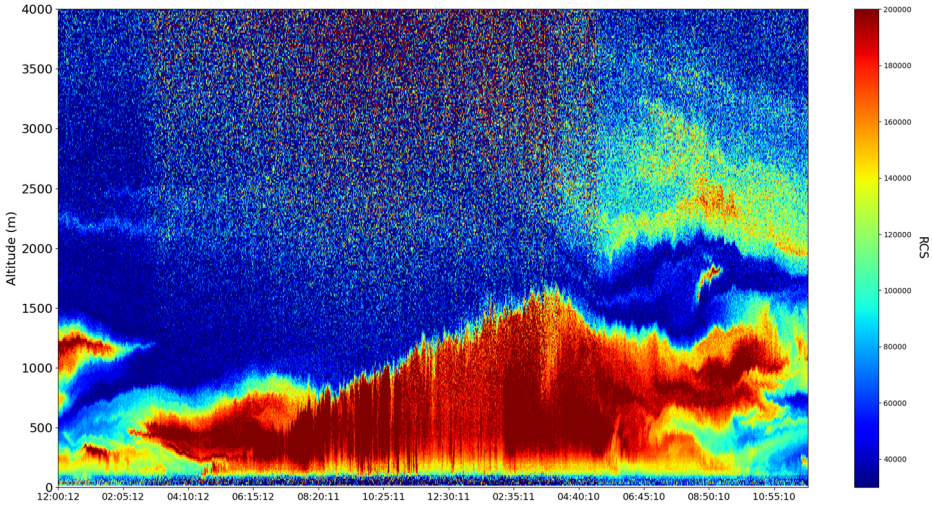

Figure 16. Time series of atmospheric RCS profiles; ceilometer data; Galati, Romania, 8 May 2022.

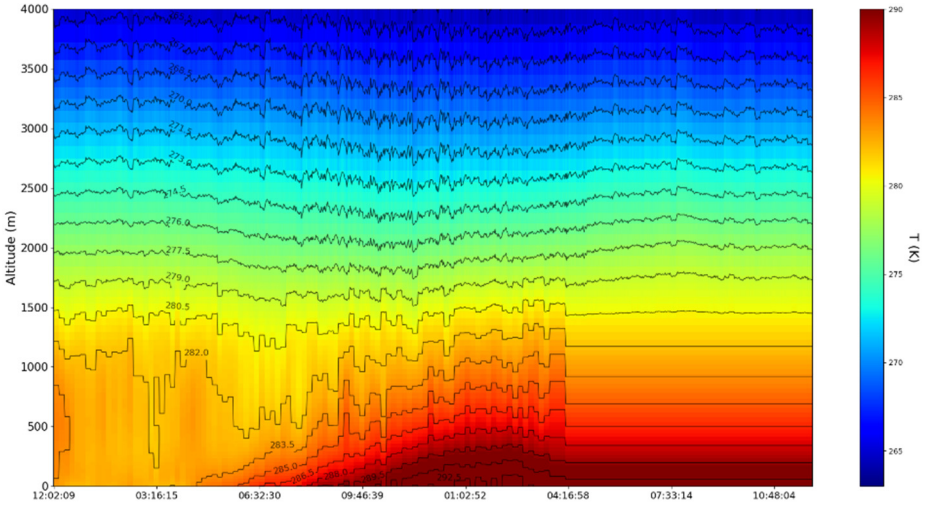

Figure 17. Time series of atmospheric temperature profiles; radiometer data; Galati, Romania, 8 May 2022.

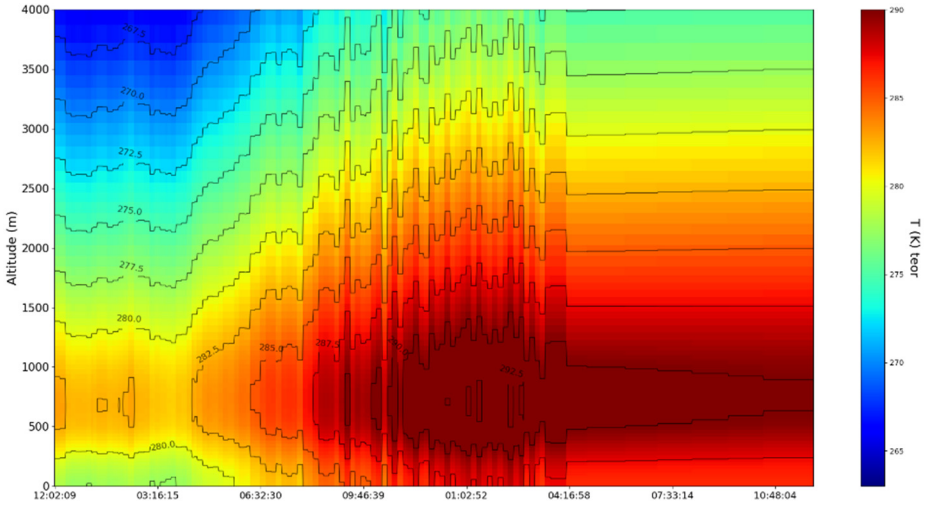

Figure 18. Time series of atmospheric temperature profiles; theoretical model data; Galati, Romania, 8 May 2022.

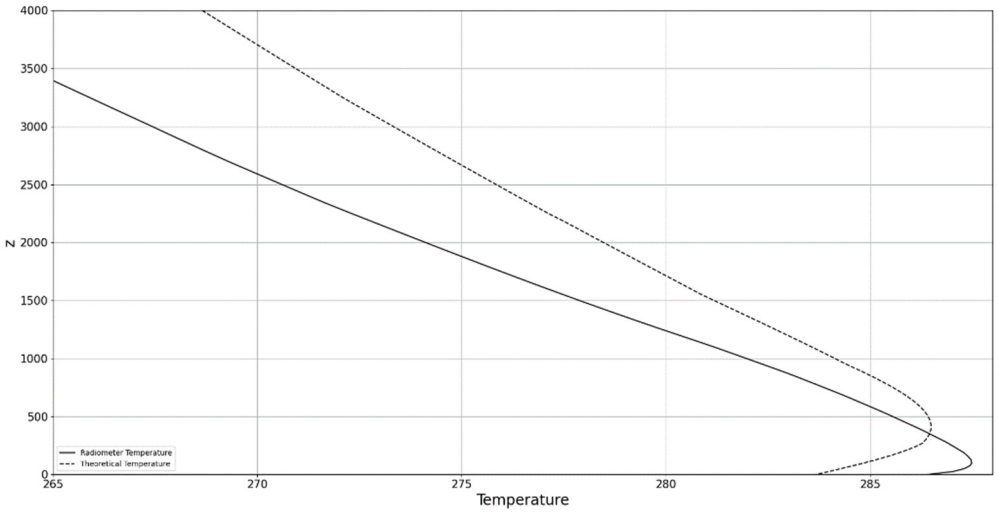

Figure 19. Profile of atmospheric temperature; radiometer data and theoretical model data; Galati, Romania, 5 May 2022; straight line: radiometer temperature; dotted line: theoretical temperature.

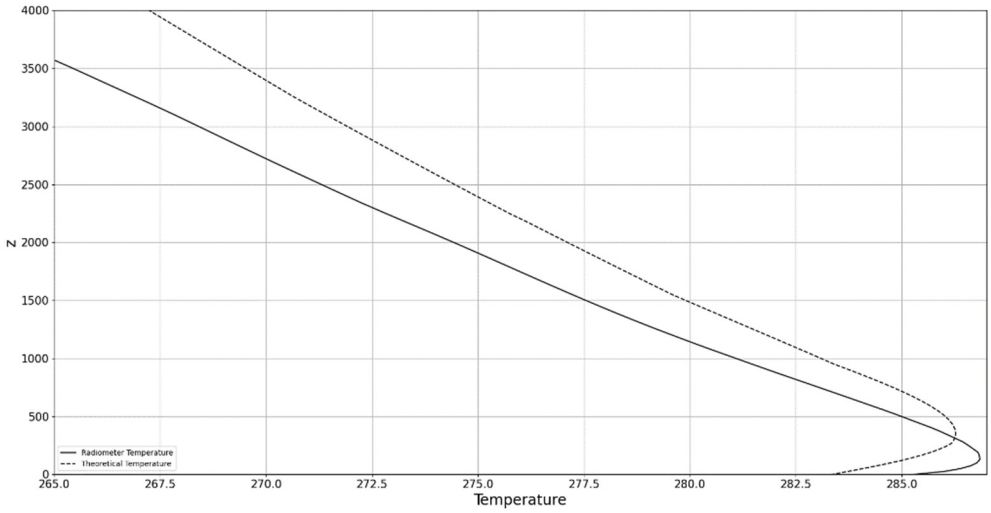

Figure 20. Profile of atmospheric temperature; radiometer data and theoretical model data; Galati, Romania, 6 May 2022; straight line: radiometer temperature; dotted line: theoretical temperature.

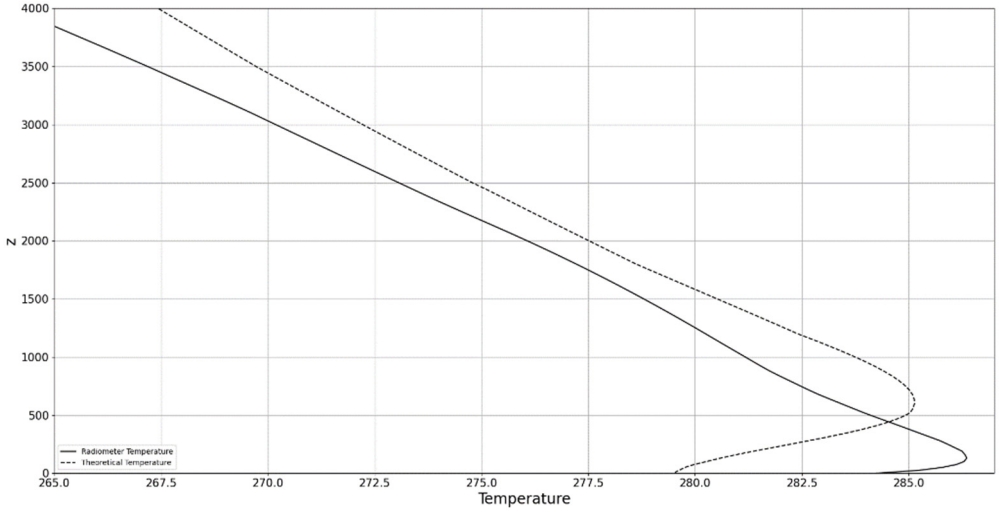

Figure 21. Profile of atmospheric temperature; radiometer data and theoretical model data; Galati, Romania, 7 May 2022; straight line: radiometer temperature; dotted line: theoretical temperature.

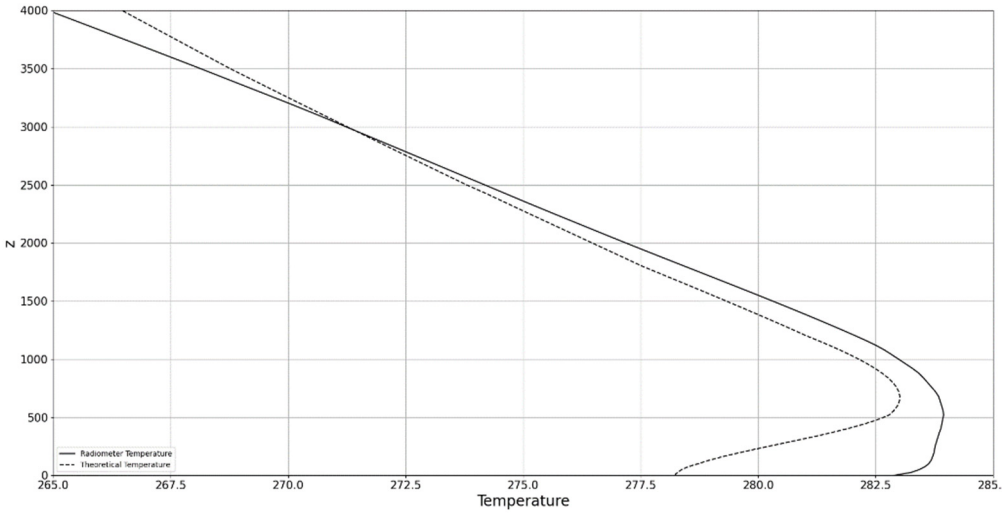

Figure 22. Profile of atmospheric temperature; radiometer data and theoretical model data; Galati, Romania, 8 May 2022; straight line: radiometer temperature; dotted line: theoretical temperature.

As can be seen in the timestamps of the time series, they all represent datasets taken for the entirety of each day, starting from midnight (Figures 7–18). The temporal resolution of the ceilometer data is one profile every minute, and the spatial resolution is 3.5 m. From the ceilometer profiles, typical low atmosphere behaviors are readily available, and the diurnal–nocturnal cycle of the PBL can be observed (Figures 7, 10, 13 and 16). To determine PBLH, a vertical spatial derivative algorithm was applied to the profiles—this well-established method, called the "gradient method", has also been compared in past studies with more current algorithms [25–27]. This PBLH is then iterated in order to produce the theoretical temperature time series as previously explained (Figures 9, 12, 14 and 18). It is found that while the theoretical time series seems to slightly overestimate the inversion and slightly underestimate the temperature lapse at higher altitudes, they are a close match to the behavior of the experimental time series (Figures 8, 9, 11–14, 17 and 18). These results point towards the fact that our multifractal interpretation has merits, meaning that the model does predict the temperature inversion and subsequent lapse throughout the atmosphere. Considering the fundamental capability of the model to properly assess the general behavior and evolution of the experimental data, it can be used in future studies as a theoretical predictor of atmospheric temperature if further adjustments are performed. For

a more precise analysis of the order differences between the experimental and theoretical temperature datasets to be performed, static profiles are shown next.

A discussion regarding the nature of temperature profiles is in order; it is known that for diurnal profiles, there exists a slightly greater decrease in temperature in the SL, and for nocturnal profiles, there is an inversion at the SL [1,28–31]. Otherwise, inversions also mark the occurrence of the PBLH [1]. In this case, solely nocturnal profiles have been chosen from the beginning of the time series. As can be seen in the temperature profile figures, the theoretical model predicts the inversion at the boundary layer, although once again, it does not always accurately predict the altitude at which the inversion takes place (Figures 19–22). This is because the model has not been adjusted to account for any surface radiative effects, merely taking into consideration the effects of the boundary layer. That being said, maximal differences between the theoretical and the experimental temperature profiles are on the order of degrees throughout the entirety of the profile; thus, it is possible to state that the model shows success in approximating both the order and the spatial evolution of the atmospheric temperature profile and iterating it with PBLH data produces satisfactory results. The slight differences between Figures 19 and 22, Figures 20 and 21 must also be highlighted—even though the order of the differences between the theoretical and real profiles seems to remain the same, the theoretical profile in Figure 22 might show a more favorable shape because of the slightly lower temperature gradient that can be found in the early segment of the dataset represented by Figure 17.

5. Conclusions

In conclusion, by employing a multifractal interpretation of atmospheric dynamics, wherein the laws that govern atmospheric motions are reliant on the notion of scale resolution, it is possible to construct the framework for atmospheric parameter behavior inversion. By considering the atmosphere from a multifractal states density perspective, the PBL, or any other atmospheric boundary layer, can be stated as a potential barrier with associated transparencies and reflectance, which directly govern the fluctuations of all multifractal atmospheric parameters. This is then found, through the use of non-dimensional plotting, to imply inversions in such parameters, including temperature. Finally, radiometer data offers various examples of atmospheric temperature inversions, wherein theoretical products made by iterating the model with PBLH data given by a ceilometer platform agree with experimental data.

Author Contributions: Conceptualization, M.M.C., I.-A.R. and M.A.; methodology, M.M.C., I.-A.R. and M.A.; software, M.M.C., I.-A.R. and M.A.; validation, M.M.C., I.-A.R. and M.A.; formal analysis, M.M.C., I.-A.R., M.A. and A.M.R.; investigation, M.M.C., I.-A.R., M.A., A.M.R. and D.V.; resources, M.M.C., I.-A.R., M.A., L.B. and D.V.; data curation, M.M.C., I.-A.R. and M.A.; writing—original draft preparation, M.M.C., I.-A.R., M.A., L.B. and D.V.; writing—review and editing, M.M.C., I.-A.R. and M.A.; visualization, M.M.C., I.-A.R. and M.A.; supervision, M.M.C. and M.A.; project administration, M.M.C., I.-A.R. and M.A.; funding acquisition, M.M.C. All authors have read and agreed to the published version of the manuscript.

Funding: This work was supported by a grant from the Romanian Ministry of Education and Research, CNCS-UEFISCDI, project number PN-III-P1-1.1-TE-2019-1921, within PNCDI III.

Institutional Review Board Statement: Not applicable.

Informed Consent Statement: Not applicable.

Data Availability Statement: The raw data supporting the conclusions of this article will be made available by the authors without undue reservation.

Acknowledgments: The authors acknowledge the UGAL–REXDAN cloud remote sensing facility, part of ACTRIS–RO (Aerosol, Clouds and Trace gases Research InfraStructure—Romania), for providing radiometer data used in this study. In addition, the authors acknowledge the RADO (Romanian Atmospheric 3D research Observatory).

Conflicts of Interest: The authors declare no conflict of interest.

References

1. Roland, S. *Practical Meteorology: An Algebra-Based Survey of Atmospheric Science*; The University of British Columbia: Vancouver, BC, Canada, 2015.
2. Badii, R.; Politi, A. *Complexity: Hierarchical Structures and Scaling in Physics*; Cambridge University Press: Cambridge, UK, 1997.
3. Mitchell, M. *Complexity: A Guided Tour*; Oxford University Press: Oxford, UK, 2009.
4. Notalle, L. *Fractal Space-Time and Microphysics*; World Scientific Publisher: Singapore, 1993.
5. Merches, I.; Agop, M. *Differentiability and Fractality in Dynamics of Physical Systems*; World Scientific Publisher: Singapore, 2015.
6. Nottale, L. *Scale Relativity and Fractal Space-Time: A New Approach to Unifying Relativity and Quantum Mechanics*; Imperial College Press: London, UK, 2011.
7. Agop, M.; Buzea, C.; Vasincu, D.; Timofte, D. Dynamics of Biostructures on a Fractal/Multifractal Space-Time Manifold. In *Progress in Relativity*; IntechOpen: London, UK, 2019; p. 117.
8. Liu, L.; Hu, F.; Huang, S. A Multifractal Random-Walk Description of Atmospheric Turbulence: Small-Scale Multiscaling, Long-Tail Distribution, and Intermittency. *Bound. Layer Meteorol.* **2019**, *172*, 351–370. [CrossRef]
9. Kalamaras, N.; Tzanis, C.G.; Deligiorgi, D.; Philippopoulos, K.; Koutsogiannis, I. Distribution of Air Temperature Multifractal Characteristics Over Greece. *Atmosphere* **2019**, *10*, 45. [CrossRef]
10. Plocoste, T.; Carmona-Cabezas, R.; Jiménez-Hornero, F.J.; de Ravé, E.G. Background PM10 atmosphere: In the seek of a multifractal characterization using complex networks. *J. Aerosol Sci.* **2021**, *155*, 105777. [CrossRef]
11. Ruelle, D.; Takens, F. On the nature of turbulence. *Les Rencontres Phys. Mathématiciens Strasbg. RCP25* **1971**, *12*, 1–44.
12. Takens, F. Detecting Strange Attractors in Turbulence. In *Dynamical Systems and Turbulence. Warwick 1980*; Springer: Berlin/Heidelberg, Germany, 1981; pp. 366–381.
13. Nottale, L. Scale relativity and fractal space-time: Applications to quantum physics, cosmology and chaotic systems. *Chaos Solitons Fractals* **1996**, *7*, 877–938. [CrossRef]
14. Nottale, L.; Auffray, C. Scale relativity theory and integrative systems biology: 2 Macroscopic quantum-type mechanics. *Prog. Biophys. Mol. Biol.* **2008**, *97*, 115–157. [CrossRef] [PubMed]
15. Chavanis, P.-H. Derivation of a generalized Schrödinger equation from the theory of scale relativity. *Eur. Phys. J. Plus* **2017**, *132*, 286. [CrossRef]
16. Roșu, I.-A.; Nica, D.-C.; Cazacu, M.M.; Agop, M. Cellular Self-Structuring and Turbulent Behaviors in Atmospheric Laminar Channels. *Front. Earth Sci.* **2022**, *9*, 801020. [CrossRef]
17. Baker, G.L.; Gollub, J.P. *Chaotic Dynamics: An Introduction*; Cambridge University Press: New York, NY, USA, 1996.
18. Ott, E. *Chaos in Dynamical Systems*; Cambridge University Press, University of Maryland: College Park, MD, USA, 2002; pp. 160–182. [CrossRef]
19. Van den Berg, J.C. *Wavelets in Physics*; Cambridge University Press: Cambridge, UK, 2004; pp. 143–147.
20. Cristescu, C.P. *Nonlinear Dynamics and Chaos Theoretical Fundaments and Applications*; Romanian Academy Publishing House: Bucharest, Romania, 2008.
21. Agop, M.; Ochiuz, L.; Tesloianu, D.; Buzea, C.; Irimiciuc, S. *Non-Differentiable Dynamics in Complex Systems*; Nova Science Publishers: New York, NY, USA, 2018.
22. Mandelbrot, B. *The Fractal Geometry of Nature*; W.H. Freeman Publishers: New York, NY, USA, 1982.
23. Barnsley, M.F. *Fractals Everywhere*; Morgan Kaufmann Publisher: San Francisco, CA, USA, 1993.
24. Bujoreanu, C.; Irimiciuc, Ş.; Benchea, M.; Nedeff, F.; Agop, M. A fractal approach of the sound absorption behaviour of materials. Theoretical and experimental aspects. *Int. J. Non-Linear Mech.* **2018**, *103*, 128–137. [CrossRef]
25. Flamant, C.; Pelon, J.; Flamant, P.H.; Durand, P. Lidar determination of the entrainment zone thickness at the top of the unstable marine atmospheric boundary layer. *Bound. Layer Meteorol.* **1997**, *83*, 247–284. [CrossRef]
26. Haeffelin, M.; Angelini, F.; Morille, Y.; Martucci, G.; Frey, S.; Gobbi, G.P.; Lolli, S.; O'Dowd, C.D.; Sauvage, L.; Xueref-Rémy, I.; et al. Evaluation of Mixing-Height Retrievals from Automatic Profiling Lidars and Ceilometers in View of Future Integrated Networks in Europe. *Bound. Layer Meteorol.* **2011**, *143*, 49–75. [CrossRef]
27. Rosu, I.-A.; Cazacu, M.-M.; Prelipceanu, O.S.; Agop, M. A Turbulence-Oriented Approach to Retrieve Various Atmospheric Parameters Using Advanced Lidar Data Processing Techniques. *Atmosphere* **2019**, *10*, 38. [CrossRef]
28. Orlanski, I.; Ross, B.B.; Polinsky, L.J. Diurnal Variation of the Planetary Boundary Layer in a Mesoscale Model. *J. Atmospheric Sci.* **1974**, *31*, 965–989. [CrossRef]
29. Hu, X.-M.; Nielsen-Gammon, J.; Zhang, F. Evaluation of Three Planetary Boundary Layer Schemes in the WRF Model. *J. Appl. Meteorol. Clim.* **2010**, *49*, 1831–1844. [CrossRef]
30. Seidel, D.J.; Ao, C.; Li, K. Estimating climatological planetary boundary layer heights from radiosonde observations: Comparison of methods and uncertainty analysis. *J. Geophys. Res. Atmos.* **2010**, *115*, 1–15. [CrossRef]
31. Wyngaard, J.C. Structure of the PBL. In *Lectures on Air Pollution Modeling*; American Meteorological Society: Boston, MA, USA, 1988; pp. 9–61.